Chinese Chemical Letters 33 (2022) 4635–4639

Contents lists available at ScienceDirect

Chinese Chemical Letters

journal homepage: www.elsevier.com/locate/cclet

Enabling ultrafast lithium-ion conductivity of Li_2ZrCl_6 by indium doping

Shuai Chen[a,b], Chuang Yu[a,*], Shaoqing Chen[c], Linfeng Peng[a], Cong Liao[a], Chaochao Wei[a], Zhongkai Wu[a], Shijie Cheng[a], Jia Xie[a,*]

[a] State Key Laboratory of Advanced Electromagnetic Engineering and Technology, School of Electrical and Electronic Engineering, Huazhong University of Science and Technology, Wuhan 430074, China
[b] School of Materials Science and Engineering, Huazhong University of Science and Technology, Wuhan 430074, China
[c] Department of Materials Science and Engineering, Southern University of Science and Technology, Shenzhen 518055, China

ARTICLE INFO

Article history:
Received 30 September 2021
Revised 7 December 2021
Accepted 20 December 2021
Available online 24 December 2021

Keywords:
Solid electrolyte
Li_2ZrCl_6
Li-ion conductivity
In-doping
Solid-state battery

ABSTRACT

Solid-state batteries with high energy density and safety are promising next-generation battery systems. However, lithium oxide and lithium sulfide electrolytes suffer low ionic conductivity and poor electrochemical stability, respectively. Lithium halide solid electrolyte shows high conductivity and good compatibility with the pristine high-voltage cathode but limited applications due to the high price of rare metal. Zr-based lithium halides with low cost and high stability possess great potential. Herein, a small amount of In^{3+} is introduced in Li_2ZrCl_6 to synthesize $Li_{2.25}Zr_{0.75}In_{0.25}Cl_6$ electrolytes with a high room temperature Li-ion conductivity of 1.08 mS/cm. Solid-state batteries using $Li_{2.25}Zr_{0.75}In_{0.25}Cl_6/Li_{5.5}PS_{4.5}Cl_{1.5}$ bilayer solid electrolytes combined with Li-In anode and pristine $LiNi_{0.7}Mn_{0.2}Co_{0.1}O_2$ cathode deliver high initial discharge capacities under different cut-off voltages. This work provides an effective strategy for enhancing the conductivity of Li_2ZrCl_6 electrolytes, promoting their applications in solid-state batteries.

Solid-state lithium batteries using Li-ion solid electrolyte have excellent potential for next-generation energy storage devices due to their better safety and higher energy density compared to the current lithium-ion batteries with organic liquid electrolytes [1–4]. Exploring lithium-ion conductors with ultrafast ionic conductivity and wide voltage windows plays a crucial role in the development of solid-state lithium batteries [5,6]. Inorganic lithium solid electrolytes include sulfides [7,8], oxides [9], polymer [10], halides [11,12], have attracted significant attention in the past years. Among those solid electrolytes, lithium oxides and lithium sulfides have been most investigated. The former shows good ionic conductivity and wide chemical/electrochemical stabilities but suffering from poor interfacial contact towards electrode materials while the latter holds ultrafast ionic conductivity and good solid-solid interfacial contact but limits due to its narrow voltage window and poor chemical/electrochemical stabilities [13–15]. Unlike oxides and sulfides, lithium halides with high ionic conductivities (10^{-3} S/cm) and good contact with electrode materials, especially high voltage compatibility towards cathode materials, show great potential as candidate solid electrolytes for constructing high energy density solid-state batteries [16–18].

Although the study of lithium halides started a long time ago, their excellent electrochemical stability towards pristine high voltage cathodes, which is one of the most attractive features, has been reported recently [19]. Asano *et al.* found that the trigonal Li_3YCl_6 and monoclinic Li_3YBr_6 with ionic conductivities of 0.51 and 1.7 mS/cm showed excellent electrochemical performances when acting as electrolytes for solid-state batteries combined with uncoated $LiCoO_2$ cathode [20]. Those electrolytes exhibited superior chemical/electrochemical stability up to 4.3 V *vs.* Li^+/Li^0. Afterward, plenty of Li-M-X compounds with room temperature ionic conductivity higher than 10^{-3} S/cm have been reported, such as Li_3InCl_6 [21,22], Li_3InBr_6 [24], Li_xScCl_{3+x} [23] and Li_3ErCl_6 [25] solid electrolytes. However, many high-cost rare metals (In, Sc and Er) in the structure limit their wide applications in solid-state batteries. Designing lithium halide electrolytes consisting of earth-abundant elements can accelerate its practical application. The monoclinic Li_2ZrCl_6 consists of low-cost Zr makes it a fantastic candidate for lithium halide electrolyte, while it suffers from poor room temperature lithium-ion conductivity (10^{-6} S/cm). Recently, Kwak et al. reported that the ionic conductivity of *hcp* Li_2ZrCl_6 could be enhanced from 0.4 mS/cm up to 1 mS/cm *via*

* Corresponding authors.
E-mail addresses: cyu2020@hust.edu.cn (C. Yu), xiejia@hust.edu.cn (J. Xie).

https://doi.org/10.1016/j.cclet.2021.12.048
1001-8417/

an aliovalent substitution of Zr^{4+} with Fe^{3+} and the modified lithium halide electrolytes showed excellent electrochemical performance towards pristine single-crystalline $LiNi_{0.88}Co_{0.11}Al_{0.01}O_2$ [26]. Although a significant increment of Li-ion conductivity has been achieved for Li_2ZrCl_6, it is a big challenge to modify this electrolyte with even higher conductivity. Moreover, the voltage stability of lithium halide electrolyte has typically been investigated till 4.3 V *vs*. Li^+/Li^0, while the cathode compatibility at an even higher voltage window is unclear. Unraveling the high voltage stability of lithium halides provides an insight viewpoint to fabricate solid-state battery utilizing high voltage cathode enables high energy density.

Zirconium is abundant in nature, and the corresponding halide electrolytes with Zr^{4+} have much lower raw-material costs than other halide electrolytes with metal in IIIA and IIIB [27]. Inspired by the previous work, we try to enhance the ionic conductivity of Li_2ZrCl_6 by introducing a small amount of In^{3+}. This work describes the strategy of improving the ionic conductivity of Li_2ZrCl_6 via indium doping. $Li_{2.25}Zr_{0.75}In_{0.25}Cl_6$ with a room temperature Li-ion conductivity of 1.08 mS/cm is successfully synthesized by the mechanical milling route. This result is consistent with the previous computational studies that the aliovalent substitution strategy effectively enhances ionic conductivity [28]. Moreover, the phase evolution and ionic conductivity variations during the milling durations have been investigated in detail. The electrochemical performance of the obtained electrolyte is evaluated by constructing solid-state batteries using pristine $LiNi_{0.7}Mn_{0.2}Co_{0.1}O_2$. Furthermore, the electrochemical stability of $Li_{2.25}Zr_{0.75}In_{0.25}Cl_6$ is investigated by cycling the assembled battery at a higher cut-off voltage window. The variations of resistance of different parts of solid-state batteries under different conditions are carefully studied *via* electrochemical impedances, which will be helpful to promote the application of lithium halide electrolytes.

The $Li_{2+x}Zr_{1-x}In_xCl_6$ are synthesized by the mechanical milling method. Raw materials LiCl (99.99% Aladdin), $InCl_3$ (99.99% Aladdin), $ZrCl_4$ (99.9% Aladdin) are mixed in proportion in 45 mL WC jars with WC balls. The weight ratio of raw materials and balls is fixed at 1:40. The mixture is ball milled (Restch, PM200) with a speed of 550 rpm after different milling durations. The $Li_{5.5}PS_{4.5}Cl_{1.5}$ electrolytes are synthesized according to our previous work [29].

X-ray diffractometer patterns are collected using Cu radiation from a Smart-Lab-SE Powder instrument over a 2θ range from 10°−80°. Scientific™ Talos F200X with four energy-dispersive X-ray spectroscopy (EDX) signal detectors are worked at 200 kV to show the signal high-resolution transmission electron microscope (HRTEM), high angle annular dark-field scanning TEM (HAADF-STEM) and elemental mapping images.

Solid-state battery fabrications: The cathode mixture is obtained by mixing the NCM712 and $Li_{2.25}Zr_{0.75}In_{0.25}Cl_6$ electrolyte with a weight ratio of 7:3. To assemble the solid-state battery, 5 mg of the cathode mixture and 80 mg of the $Li_{2.25}Zr_{0.75}In_{0.25}Cl_6$ electrolyte are pressed together to form a bilayer pellet. Then, 30 mg of $Li_{5.5}PS_{4.5}Cl_{1.5}$ is chosen to add on the surface of the other side to separate the direct contact of halide electrolyte and In-Li anode. After that, the triple-layer pellet is pressed together under 380 MPa for 1 min using cold-pressing. Finally, the In-Li alloy is attached to the $Li_{5.5}PS_{4.5}Cl_{1.5}$ layer side under the pressure of 150 MPa. All those fabrication processes are operated in an argon-filled glovebox (O_2, $H_2O < 0.1\%$).

Electrochemical characterizations: 100 mg of the obtained electrolytes power are pressed under 380 MPa for 1 min in the model cell using stainless steel disks as the blocking electrodes. Alternating current impedance is measured in the frequency range between 0.1 Hz and 1 MHz with an applied voltage of 0.02 V at different temperatures for the solid electrolyte pellets and the cycled solid-state batteries. The assembled solid-state batteries are charged/discharged at 0.2 C with different voltage windows (3.0 ~4.3 V and 3.0~4.5 V) under different temperatures (room temperature and 60 °C) using a charge-discharge measurement device from Neware (CT4008). *In-situ* EIS are operated with Bio-Logic SP-300 in the frequency range between 0.1 Hz and 6 MHz with an applied voltage of 0.02 V.

The typical mechanical milling synthetic route was chosen to prepare the pristine Li_2ZrCl_6 and indium-doped materials. XRD patterns are measured to show the phase transitions with increasing In^{3+} proportions. As shown in Fig. 1a, the XRD patterns of these pristine materials are indexed to the trigonal Li_3YCl_6 structure with a space group of *p3m1*. With increasing x ratio of $Li_{2+x}Zr_{1-x}In_xCl_6$, the intensities of diffraction peaks located at ~30° and ~34° become stronger, and the intensities of XRD peaks at ~16°, ~30°, and ~41° are obviously reduced, which can be interpreted as a phase transition effect by the aliovalent substitution of In^{3+} in the structure. When x values are higher than 0.4, the obtained samples exhibit a complete phase transition to the monoclinic Li_3InCl_6 structure with a space group of *C2/m*. In Fig. 1b, the modified solid electrolyte with the composition of $x = 0.25$ exhibits the lowest resistance of 59.5 Ω among solid electrolytes with different dopant amounts. In Fig. 1c, the room temperature Li-ion conductivities are 0.63 mS/cm for $x = 0.10$, 0.72 mS/cm for $x = 0.20$, 1.08 mS/cm for $x = 0.25$, 0.81 mS/cm for $x = 0.30$, 0.5 mS/cm for $x = 0.40$, 0.43 mS/cm for $x = 0.50$, respectively. $Li_{2.25}Zr_{0.75}In_{0.25}Cl_6$ delivers the highest ionic conductivity among those different compositions. Ionic conductivities of those electrolytes at different temperatures are also tested, as shown in Fig. 1d. The corresponding activation energies can be deduced from the Arrhenius plots in Fig. 1d. The optimal $Li_{2.25}Zr_{0.75}In_{0.25}Cl_6$ shows the smallest activation energies of 0.29 eV among those different compositions (Fig. 1e), which agrees well with the ionic conductivity variations.

Fig. 2a shows the XRD diffractions of the mixture obtained by milling the starting materials (LiCl, $InCl_3$ and $ZrCl_4$) with the rotation speed of 550 rpm from 2 h to 16 h. For the mixture obtained after 110 rpm milling for 1 h, strong diffraction peaks are indexed to the standard reflection peaks of those starting materials, suggesting that this process slightly influences the phase transition during the synthesis. Then, the milling speed was increased to 550 rpm, and the mill jar was opened every 2 h to make sure that the mixture was homogenous during the high rotation process. The major diffraction peaks of the mixtures in Fig. 2a are indexed to the hcp trigonal Li_3YCl_6 structure with a space group of *p3m1* after 2 h of milling. With longer milling durations, no obvious additional reflection can be observed in the XRD patterns, suggesting that pure trigonal $Li_{2.25}Zr_{0.75}In_{0.25}Cl_6$ was successfully prepared *via* a directly mechanical milling process. The milling duration plays a crucial role in the Li-ion conductivity of the obtained electrolytes. Therefore, the variation of conductivities as a function of milling durations are carefully investigated during the synthetic process for $Li_2Zr_{0.75}In_{0.25}Cl_6$ electrolyte. After the low-speed mixing process (110 rpm/1 h), the homogenous mixed raw materials show a very low conductivity out of the impedance limit.

During the subsequent high rotation milling durations, the ionic conductivity of the mixture exhibits a rapid increment in the first six hours from 0.33 mS/cm to 0.91 mS/cm, while it shows slight changes in the next 10 h. The milled mixture delivers Li-ion conductivities of 1.02, 1.05, and 1.08mS/cm after 8, 12 and 16 h of milling durations (Fig. 2b), respectively. As shown in Fig. 2c, the resistance for the milled Li_2ZrCl_6 and $Li_{2.25}Zr_{0.75}In_{0.25}Cl_6$ electrolytes are 224 and 51.7 Ω, corresponding to Li-ion conductivities of 0.32 mS/cm and 1.08 mS/cm at ambient temperatures (Fig. 2d), respectively. After introducing a minor amount of indium in the structure of Li_2ZrCl_6, the Li-ion conductivity is nearly four folders higher than that of the pristine material, indicating that in-

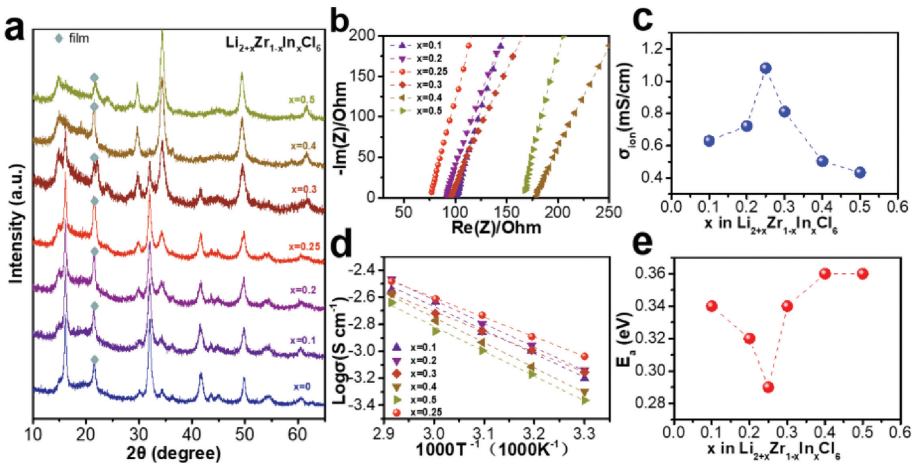

Fig. 1. (a) XRD patterns of the $Li_{2+x}Zr_{1-x}In_xCl_6$. (b) Room temperature complex resistance plot for Li_2ZrCl_6 electrolytes with various amount of In^{3+} doping and (c) corresponding ionic conductivity. (d) Arrhenius plots of the different In^{3+} introducing samples and (e) corresponding activation energies.

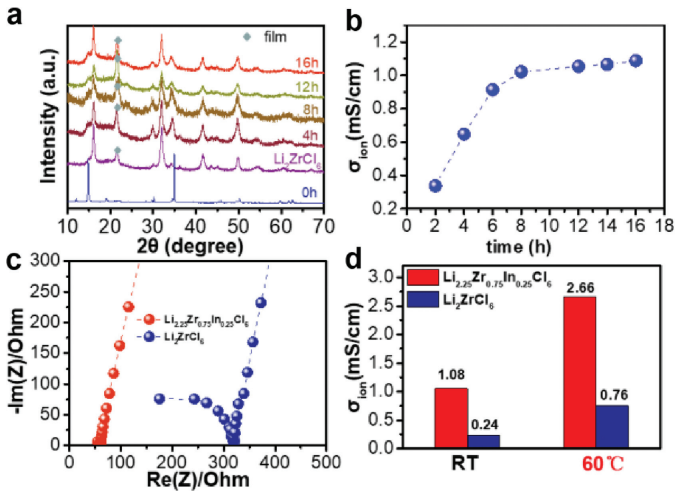

Fig. 2. (a) XRD patterns of the mixture of raw materials LiCl, $InCl_3$, and $ZrCl_4$ milled with 500 rpm for various durations. (b) The corresponding variations of Li-ion conductivity for the milled mixture as a function of milling time. (c) Room temperature complex impedance plots of Li_2ZrCl_6 and $Li_{2.25}Zr_{0.75}In_{0.25}Cl_6$ solid electrolytes obtained by mechanical milled at 500 rpm for 16 h. (d) Li-ion conductivities of the milled Li_2ZrCl_6 and $Li_{2.25}Zr_{0.75}In_{0.25}Cl_6$ solid electrolytes. Stainless steel was chosen as the blocking electrode.

dium doping is an effective solution to enhance the conductivity of Li_2ZrCl_6.

Due to the poor crystallinity of solid electrolytes obtained *via* the mechanical milling route, the subsequent heat treatment process significantly affects the ionic conductivity [30]. To investigate the annealing effect on the phase transitions and ionic conductivity of $Li_{2.25}Zr_{0.75}In_{0.25}Cl_6$ electrolyte, the milled material was annealed at different chosen temperatures. As shown in Fig. 3a, the reflections of $Li_{2.25}Zr_{0.75}In_{0.25}Cl_6$ after sintered at 210 and 310 °C are indexed to Li_3InCl_6 phase with the space group of C2/m. The sharper diffraction peaks for the annealed $Li_{2.25}Zr_{0.75}In_{0.25}Cl_6$ suggests an improved crystallinity. Fig. 3b depicts the complex impedance plots for the annealed $Li_{2.25}Zr_{0.75}In_{0.25}Cl_6$ electrolytes. The resistances are 105 and 92.5 Ω for $Li_{2.25}Zr_{0.75}In_{0.25}Cl_6$ sintered at 210 and 310 °C, respectively, both of which are higher than that of the milled sample (51.7 Ω). The corresponding room temperature Li-ion conductivities are 0.75 and 0.69 mS/cm, respectively, much lower than that of the milled $Li_{2.25}Zr_{0.75}In_{0.25}Cl_6$ (1.08 mS/cm). Moreover, as shown in Fig. 3c, $Li_{2.25}Zr_{0.75}In_{0.25}Cl_6$ annealed at 310 °C delivers slightly lower ionic conductivities than that of the one annealed at 210 °C under different measuring temperatures. Both annealed samples exhibit much smaller conductivities than the milled $Li_{2.25}Zr_{0.75}In_{0.25}Cl_6$. It appears that although the heat treatment process increases the crystallinity, it also reduces the Li-ion conductivity due to the phase translation of crystal structure [24].

Transmission electron microscope (TEM) observations and EDX are carried out to clarify the microstructure of the $Li_{2.25}Zr_{0.75}In_{0.25}Cl_6$ electrolyte before and after heat treatment. As displayed in Fig. 3d, the high-resolution TEM image of the $Li_{2.25}Zr_{0.75}In_{0.25}Cl_6$ electrolyte prepared by ball-milling shows a disorder structural, and the EDX mapping demonstrates the uniform dispersion of Zr, In, Cl elements in the electrolyte. Fig. 3e shows the high-resolution TEM image of the $Li_{2.25}Zr_{0.75}$ $In_{0.25}Cl_6$ electrolyte after heat treatment at 210 °C, which indicates a coexistence state of lowly crystalline phase and amorphous phase. The crystalline phase shows lattice fringes of ~0.60 nm, corresponding to 14.75° of the (001) plane in the XRD patterns. The STEM images and EDX mappings indicate the uniform dispersion of Zr, In, Cl elements in the prepared solid electrolytes. These results suggest that heat treatment can significantly improve the crystallinity of $Li_{2.25}Zr_{0.75}In_{0.25}Cl_6$ electrolytes without destroying the element distribution.

To investigate the compatibility of the milled $Li_{2.25}Zr_{0.75}$ $In_{0.25}Cl_6$ towards Li-In anode, $LiNi_{0.7}Mn_{0.2}Co_{0.1}O_2$/$Li_{2.25}Zr_{0.75}$ $In_{0.25}Cl_6$/Li-In solid-state batteries were fabricated and the corresponding impedance spectra as a function of storage durations were performed. Fig. S1a (Supporting information) shows unchanged resistance due to the solid electrolyte and large variations of interface resistance, which is associated with the instability of $Li_{2.25}Zr_{0.75}In_{0.25}Cl_6$ electrolyte towards pristine $LiNi_{0.7}Mn_{0.2}$ $Co_{0.1}O_2$ cathode and Li-In anode. To unravel the compatibility of $Li_{2.25}Zr_{0.75}In_{0.25}Cl_6$ towards electrode materials, $Li_{5.5}PS_{4.5}Cl_{1.5}$ was introduced as a buffer layer to separate the direct contact between the electrolyte and Li-In anode. $LiNi_{0.7}Mn_{0.2}Co_{0.1}O_2$ /$Li_{2.25}Zr_{0.75}In_{0.25}Cl_6$/$Li_{5.5}PS_{4.5}Cl_{1.5}$/In-Li solid-state battery was fabricated and the resistance variations as a function of storage durations were carefully investigated. As previously reported, lithium argyrodite solid electrolytes show excellent chemical electrochemical stability with In-Li anode [31]. Fig. S1b (Supporting information) shows minor resistance changes during the whole test process, indicating good stability between $Li_{2.25}Zr_{0.75}In_{0.25}Cl_6$ electrolyte and bare $LiNi_{0.7}Mn_{0.2}Co_{0.1}O_2$ active material. Therefore, $Li_{2.25}Zr_{0.75}In_{0.25}Cl_6$ electrolyte shows incompatibility with Li-In anode.

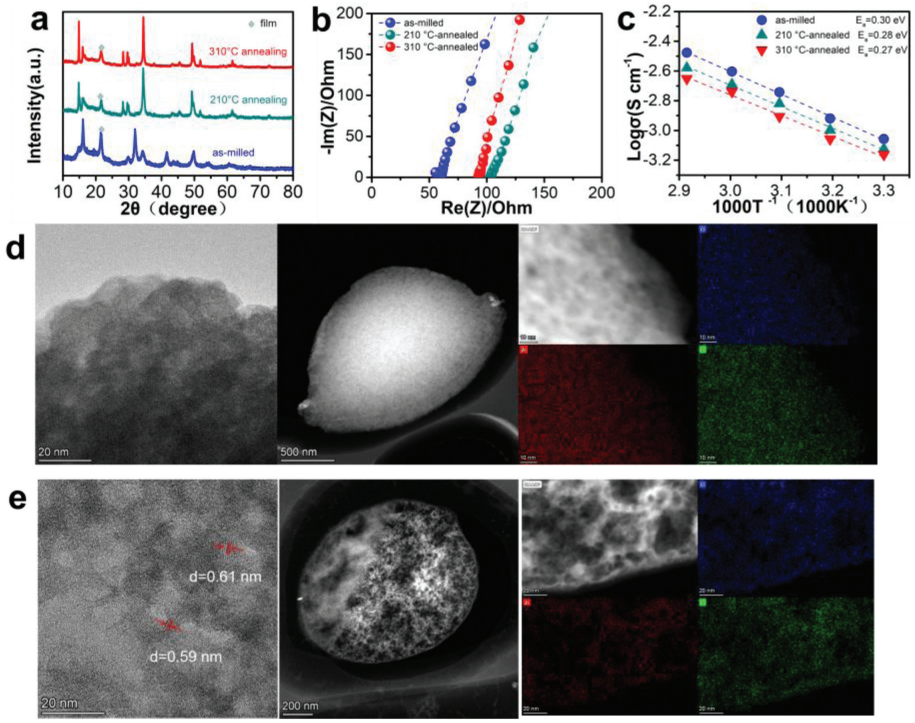

Fig. 3. (a) XRD patterns of the mixture milled at 16 h and the samples after annealing at different temperatures. (b) Complex impedance plots for $Li_{2.25}Zr_{0.75}In_{0.25}Cl_6$ annealed at 210 and 310 °C. (c) Arrhenius plots of the milled and annealed samples. TEM and EDX mapping images of (d) the milled and (e) annealed $Li_{2.25}Zr_{0.75}In_{0.25}Cl_6$.

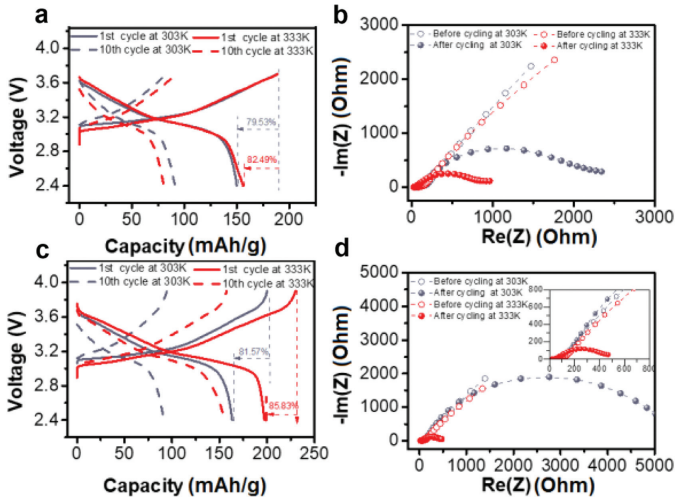

Fig. 4. Electrochemical performances evaluation of the $LiNi_{0.7}Mn_{0.2}Co_{0.1}O_2$ /$Li_{2.25}Zr_{0.75}In_{0.25}Cl_6$/$Li_{5.5}PS_{4.5}Cl_{1.5}$/Li-In solid-state batteries cycled at 0.2 C under different conditions. (a) The 1st and 10th charge/discharge curves and (b) EIS before and after cycling for the battery cycled between 3.0 V and 4.3 V at room temperature and 60 °C. (c) The 1st and 10th charge/discharge curves and (d) EIS before and after cycling for a wider voltage window of 3.0 ~ 4.5 V *vs.* Li^+/Li^0 under the same operating temperatures.

To investigate the electrochemical performances of the designed $Li_{2.25}Zr_{0.75}In_{0.25}Cl_6$, $LiNi_{0.7}Mn_{0.2}Co_{0.1}O_2$/$Li_{2.25}Zr_{0.75}In_{0.25}Cl_6$/$Li_{5.5}PS_{4.5}Cl_{1.5}$/In-Li solid-state battery was constructed. As shown in Fig. 4a, the assembled battery delivers an initial discharge capacity of 150.0 mAh/g with a coulombic efficiency of 79.5% under 0.2 C between the voltage window of 3.0–4.3 V *vs.* Li^+/Li^0 at room temperature. The discharge capacity quickly degrades below 82.8 mAh/g within 10 cycles. This poor cyclability is due to the rapid increase of $Li_{2.25}Zr_{0.75}In_{0.25}Cl_6$/$Li_{5.5}PS_{4.5}Cl_{1.5}$ electrolyte interface resistance in the middle frequency range during the first 10 cycles, as shown in Fig. 4b. The ionic conductivity of solid electrolytes is significantly influenced by the temperature, a higher temperature yields faster lithium-ion mobility. When the operating temperature increase to 60 °C, the solid-state battery shows a slightly larger initial discharge capacity of 155.0 mAh/g and higher coulombic efficiency of 82.5% and retains 88.0 mAh/g after 10 cycles (Fig. 4a). EIS results confirm that smaller solid electrolyte associated interface resistances are achieved due to the increased operating temperatures (Fig. 4b). Furthermore, the fabricated solid-state battery was also charged/discharged at a higher voltage window, between 3.0 and 4.5 V. It delivers a higher initial discharge capacity than that at a narrower voltage window, as shown in Fig. 4c. A new charge plateau is observed at 4.3 V *vs.* Li^+/Li^0, which may be associated with the side reaction between the active material and $Li_{2.25}Zr_{0.75}In_{0.25}Cl_6$. EIS results show a much larger cathode/solid electrolyte resistance in the same cycles due to the intense side reaction at a higher voltage window. $Li_{2.25}Zr_{0.75}In_{0.25}Cl_6$-based solid-state batteries show higher initial coulombic efficiencies at elevated temperature than at room temperature in different voltage windows, which may be attributed to the faster ionic mobility of the solid electrolyte. The faster lithium-ion migration rate in the cathode mixture due to the higher operating temperature can improve the reversibility, yielding enhanced coulombic efficiencies. Finally, to unravel the fast degradation of discharge capacities for the $LiNi_{0.7}Mn_{0.2}Co_{0.1}O_2$/$Li_{2.25}Zr_{0.75}In_{0.25}Cl_6$/$Li_{5.5}PS_{4.5}Cl_{1.5}$/Li-In solid-state batteries, *in-situ* EIS was applied to evaluate resistance evolutions of the assembled battery during the first two cycles operating at the same conditions. As shown in Fig. S2 (Supporting information), the resistance in the high frequencies assigned to the contribution of $Li_{2.25}Zr_{0.75}In_{0.25}Cl_6$ electrolyte shows minor variations during the charge/discharge process of the first two cycles. In contrast, the semicircle sections in the middle and low frequencies reflect the total interface resistances, including

cathode/$Li_{2.25}Zr_{0.75}In_{0.25}Cl_6$, $Li_{2.25}Zr_{0.75}In_{0.25}Cl_6/Li_{5.5}PS_{4.5}Cl_{1.5}$, and Li-In/$Li_{5.5}PS_{4.5}Cl_{1.5}$ interfaces, show intense variations during the initial charge process. The interfacial resistance appears when the battery is charged from 3.0 V to 3.3 V and significantly increases during the subsequent initial charge process till 3.7 V. During the first discharge process, the battery displays reduced interface resistance from 3.7 V to 3.0 V. Moreover, this battery exhibits much higher interfacial resistances during the 2nd charging process compared with the 1st charge process, suggesting a continuous interface degradation. As shown in Figs. S3a–d (Supporting information). A solid-state battery using $LiNbO_3$-coated $LiNi_{0.7}Mn_{0.2}Co_{0.1}O_2$ cathode and bilayer solid electrolyte layers was also constructed and showed similar fast degradation of capacity and large increase of interface resistance during cycling, indicating that the instability comes from the $Li_{2.25}Zr_{0.75}In_{0.25}Cl_6/Li_{5.5}PS_{4.5}Cl_{1.5}$ layer during cycling [32]. As shown in Fig. S4 (Supporting information), the halide electrolyte layer and $Li_{2.25}Zr_{0.75}In_{0.25}Cl_6/Li_{5.5}PS_{4.5}Cl_{1.5}$ interface are easy to craze, which show an intense mechanical incompatibility.

In summary, we have demonstrated that the ionic conductivity of low-cost Li_2ZrCl_6 solid electrolytes can be effectively enhanced via introducing indium into the structure. $Li_{2.25}Zr_{0.75}In_{0.25}Cl_6$ electrolyte was successfully synthesized through a direct mechanical milling route. It delivers a room temperature ionic conductivity of 1.08 mS/cm, four times higher than the pristine Li_2ZrCl_6, and a subsequent annealing process degrades the ionic conductivity of Li_2ZrCl_6. Solid-state batteries using the prepared $Li_{2.25}Zr_{0.75}In_{0.25}Cl_6$ electrolyte and $Li_{5.5}PS_{4.5}Cl_{1.5}$ buffer layer combined with pristine $LiNi_{0.7}Mn_{0.2}Co_{0.1}O_2$ cathode and Li-In alloy showed a high initial discharge capacity of 150.0 mAh/g at 0.2 C under room temperature when the upper cut-off voltage was 4.3 V. Discharge capacity and coulombic efficiency of solid-state battery during the initial cycle increase as a function of the increasing upper cut-off voltage and operating temperature. This battery suffers rapid capacity degradation due to the increased interface resistance of the $Li_{2.25}Zr_{0.75}In_{0.25}Cl_6/Li_{5.5}PS_{4.5}Cl_{1.5}$ layer during cycling. This work provides an effective route to enhance the ionic conductivity of halide solid electrolyte for solid-state batteries.

Declaration of competing interest

The authors declare that they have no known competing financial interests or personal relationships that could have appeared to influence the work reported in this paper.

Acknowledgments

This work was supported by the National Natural Science Foundation of China (Nos. 52177214, 51821005), the Department of Science and Technology of Guangdong Province (No. 2017ZT07Z479) and the Pico Center at SUSTech CRF that receives support from Presidential fund and Development and Reform Commission of Shenzhen Municipality. We gratefully acknowledg the Analytical and Testing Center of HUST for allowing us to use its facilities and the technical support from SUSTech CRF.

Supplementary materials

Supplementary material associated with this article can be found, in the online version, at doi:10.1016/j.cclet.2021.12.048.

Reference

[1] J. Janek, W.G. Zeier, Nat. Energy. 1 (2016) 16141.
[2] A. Manthiram, X. Yu, S. Wang, Nat. Rev. Mater. 2 (2017) 16103.
[3] C.Z. Ke, F. Liu, Z.M. Zheng, et al., Rare Met. 40 (2021) 1347–1356.
[4] Q. Yu, K. Jiang, C. Yu, et al., Chin. Chem. Lett. 32 (2021) 2659–2678.
[5] J.C. Bachman, S. Muy, A. Grimaud, et al., Chem. Rev. 116 (2016) 140–162.
[6] J. Park, J.Y. Kim, D.O. Shid, et al., Chem. Eng. J. 391 (2020) 123528.
[7] N. Kamayan, K. Homma, Y. Yamakawa, et al., Nat. Mater. 10 (2011) 682–686.
[8] Z.Y. He, Z.Q. Zhang, M. Yu, et al., Rare Met. 41 (2022) 798–805.
[9] R. Murugan, V. Thangadurai, W. Weppner, Angew. Chem. Int. Ed. 46 (2007) 7778–7781.
[10] M. Weiss, F.J. Simon, M.R. Busche, et al., Energy Rev. 3 (2020) 221–238.
[11] Z. Liu, S. Ma, J. Liu, et al., ACS Energy Lett. 6 (2020) 298–304.
[12] X. Li, J. Liang, K.R. Adair, et al., Nano Lett. 20 (2020) 4384–4392.
[13] F. Han, T. Gao, Y. Zhu, et al., Adv. Mater. 27 (2015) 3473–3483.
[14] B.R. Shin, Y.J. Nam, D.Y. Oh, et al., Electrochim. Acta 146 (2014) 395–402.
[15] M. Kotobuki, H. Mumakata, K. Kanamura, et al., J. Electrochem. Soc. 157 (2010) A1076.
[16] X. Li, J. Liang, X. Yang, et al., Energy Environ. Sci. 13 (2020) 1429–1461.
[17] H.T. Ren, Z.Q. Zhang, J.Z. Zhang, et al., Rare Met. 41 (2021) 106–114.
[18] S. Lou, F. Zhang, C. Fu, et al., Mater. Res. Bull. 33 (2021) 2000721.
[19] L. Hanebali, T. Machej, C. Cros, et al., Mater. Res. Bull. 16 (1981) 887–901.
[20] T. Asano, A. Sakai, S. Ouchi, et al., Adv. Mater. 30 (2018) e1803075.
[21] X. Li, J. Liang, J. Luo, et al., Energy Environ. Sci. 12 (2019) 2665–2671.
[22] X. Li, J. Liang, N. Chen, et al., Angew. Chem. Int. Ed. 58 (2019) 16427–16432.
[23] J. Liang, X. Li, S. Wang, et al., J. Am. Chem. Soc. 142 (2020) 7012–7022.
[24] K. Yamada, K. Kumano, T. Okuda, Solid State Ion. 177 (2006) 1691–1695.
[25] R. Schlem, S. Muy, N. Prinz, et al., Adv. Energy Mater. 10 (2020) 1903719.
[26] H. Kwak, D. Han, J. Lyoo, et al., Adv. Energy Mater. 11 (2021) 2003190.
[27] K. Wang, Q. Ren, Z. Gu, et al., Nat. Commun. 12 (2021) 4410.
[28] K. Kim, D. Park, H.G. Jung, et al., Chem. Mater. 33 (2021) 3669–3677.
[29] L. Peng, C. Yu, Z. Zhang, et al., Chem. Eng. J. 430 (2022) 132896.
[30] J. Liang, X. Li, K.R. Adair, et al., Acc. Chem. Res. 54 (2021) 1023–1033.
[31] X. Liang, Q. Pang, I.R. Kochetkov, et al., Nat. Energy 2 (2017) 17119.
[32] L. Peng, H. Ren, J. Zhang, et al., Energy Stor. Mater. 43 (2021) 53–61.